Original Paper

An approximate analytical model for unconventional reservoir considering variable matrix blocks and simultaneous matrix depletion

Kai-Xuan Qiu [a], Jia Li [b], Dong Feng [c], Shi-Ming Wei [d, *], Gang Lei [e, f, **]

[a] Jiangmen Laboratory of Carbon Science and Technology, Jiangmen, 529100, Guangdong, China
[b] The Hong Kong University of Science and Technology (Guangzhou), Guangzhou, 511400, Guangdong, China
[c] China University of Geosciences (Beijing), Beijing, 100083, China
[d] China University of Petroleum (Beijing), Beijing, 102249, China
[e] China University of Geosciences (Wuhan), Wuhan, 430074, Hubei, China
[f] Shenzhen Research Institute, China University of Geosciences, Shenzhen, 518063, Guangdong, China

A R T I C L E   I N F O

A B S T R A C T

In regard to unconventional oil reservoirs, the transient dual-porosity and triple-porosity models have been adopted to describe the fluid flow in the complex fracture network. It has been proven to cause inaccurate production evaluations because of the absence of matrix—macrofracture communication. In addition, most of the existing models are solved analytically based on Laplace transform and numerical inversion. Hence, an approximate analytical solution is derived directly in real-time space considering variable matrix blocks and simultaneous matrix depletion.

To simplify the derivation, the simultaneous matrix depletion is divided into two parts: one part feeding the macrofractures and the other part feeding the microfractures. Then, a series of partial differential equations (PDEs) describing the transient flow and boundary conditions are constructed and solved analytically by integration. Finally, a relationship between oil rate and production time in real-time space is obtained.

The new model is verified against classical analytical models. When the microfracture system and matrix—macrofracture communication is neglected, the result of the new model agrees with those obtained with the dual-porosity and triple-porosity model, respectively. Certainly, the new model also has an excellent agreement with the numerical model. The model is then applied to two actual tight oil wells completed in western Canada sedimentary basin. After identifying the flow regime, the solution suitably matches the field production data, and the model parameters are determined. Through these output parameters, we can accurately forecast the production and even estimate the petrophysical properties.
© 2023 The Authors. Publishing services by Elsevier B.V. on behalf of KeAi Communications Co. Ltd. This is an open access article under the CC BY-NC-ND license (http://creativecommons.org/licenses/by-nc-nd/4.0/).

1. Introduction

In the last decades, multifractured horizontal wells (MFHWs) have been widely used to efficiently develop unconventional oil/gas reservoirs. The ultralow permeability matrix block can be broken into smaller pieces and thus the contact area between matrix and fractures could be enhanced to achieve economic production rate. However, it remains challenging to study the fluid flow and carry out production prediction in such complex reservoirs (Wang and Ayala, 2020; Wu et al., 2021).

Generally, an analytical model began with paper from Barenblatt et al. (1960) has laid the foundation for flow analysis in a dual-porosity system. Subsequently, many analytical models (Warren and Root, 1963; Kazemi, 1969; De Swaan, 1976) have been proposed to analyze the fluid flows from the low-permeability matrix into a high-permeability fracture network based on the assumption of pseudosteady-state and transient state. With the development of unconventional reservoirs, the half-slope line on a log-log plot representing the transient linear behavior can be observed to last for a longer period. El-Banbi (1998) extended the previous basic dual-porosity models to develop a series of

* Corresponding author.
** Corresponding author.
E-mail addresses: we_shiming@163.com (S.-M. Wei), lg1987cup@126.com (G. Lei).

Nomenclature		q_{m2_Mi}	The interporosity-flow between submatrix m2 and microfractures, STB/d
c_t	Total compressibility, psi^{-1}	T_{Ff}	Transmissibility between macrofractures and microfractures, STB/d/psi
J_F	Productivity index, STB/d/psi		
P_f	Pressure in microfracture, psi	T_{Fm1}	Transmissibility between submatrix m1 and macrofractures, STB/d/psi
P_F	Pressure in macrofracture, psi		
P_{m1}	Ppressure in submatrix m1, psi	T_{fm2}	Transmissibility between submatrix m2 and microfractures, STB/d/psi
P_{m2}	Pressure in submatrix m2, psi		
q_{Fi}	Initial rate from the macrofractures, Mscf/d	μ	Fluid viscosity, cP
q_{fi}	Initial rate from the microfractures, Mscf/d	ϕ	Porosity
q_{m1i}	Initial rate from submatrix m1, Mscf/d	τ_f	Constant time in microfractures, day
q_{m2i}	Initial rate from submatrix m2, Mscf/d	τ_F	Constant time in macrofractures, day
q_{m1_Ma}	The interporosity-flow between submatrix m1 and macrofractures, STB/d	τ_{m1}	Constant time in submatrix m1, day
		τ_{m2}	Constant time in submatrix m1, day

analytical solutions considering transient linear flow in tight reservoirs. Bello (2009) established asymptotic analysis equations for different flow regimes. Later, many researchers realized improvements to the dual-porosity transient linear flow model (Brown et al., 2011; Stalgorova and Mattar, 2012, 2013; Behmanesh et al., 2017; Wu et al., 2019; Qiu, 2023). Considering that complex fracture network containing multiple types of fractures emerge after hydraulic fracturing, the dual-porosity models may not be applicable in reality.

The more comprehensive triple-porosity models encompassing either two fracture networks and one matrix or two types of matrices and one fracture network were developed recently. Abdassah and Ershaghi (1986) proposed a dual-matrix triple-porosity model for pressure transient analysis. In most cases, natural fracture or microfracture is considered as the third type of media. Al-Ghamdi and Ershaghi (1996) proposed a dual-fracture triple-porosity model consisting of pseudosteady-state linear flow behavior. Dreier (2004) improved the triple-porosity model by considering transient flow conditions between micro- and macrofractures. Then, Ahmadi (2010) and Samandarli (2012) formulated asymptotic equations for different flow regions based on the triple-porosity model, which are more beneficial for history matching and production prediction in unconventional reservoirs. Based on previous works, more innovative models for triple-porosity system have been studied (Dehghanpour and Shirdel, 2011; Tivayanonda, 2012; Lu et al., 2021; Ali et al., 2013; Wei et al., 2019; Wu et al., 2023).

The existing transient dual-porosity and triple-porosity models for unconventional fractured horizontal wells were derived based on the assumption of sequential depletion. Namely, the most common flow hierarchy is defined as: matrix to fractures to wellbore (dual-porosity model) or matrix to microfractures to macrofractures then to wellbore (triple-porosity model) sequentially. Because the communication between the matrix and macrofracture is neglected in previous studies, the properties of fractures will be estimated unreasonably especially for the situation where the matrix−macrofractures communication is significant. Therefore, a quadrilinear flow model (Ezulike and Dehghanpour, 2014) has been proposed to extend the sequential-depletion assumption to simultaneous matrix depletion. However, all of these analytical solutions were derived by Laplace transformation, which is relatively complicated due to the dimensionless transform, Laplace-transform and numerical inversion operation.

In this work, we derive an approximate analytical solution in real-time space based on simultaneous matrix-fracture flow bypassing the Laplace transformation and numerical inversion. Firstly, the mathematical model representing three interacting media are constructed based on the defined physical model and model assumptions. Secondly, the constructed mathematical model is solved analytically and then is verified against numerical model and two classical analytical solutions. Finally, the proposed model is used for production prediction purposes.

2. Methodology

2.1. Model description

To produce oil/gas from unconventional reservoirs economically, multi-stage fractured horizontal well technology has been applied commonly in petroleum industry. In the massive fracturing process, the tight matrix in production formations is broken into smaller blocks and a large amount of microfractures are created around hydraulic fractures which serve as major flow path connecting the matrix and hydraulic fractures. Generally, the generated matrix blocks must be non-uniform and have different size. To describe the flow process in such fractured reservoir, the heterogeneity of matrix cannot be ignored in mathematical models. Furthermore, the size of matrix blocks is varied with the distance from the hydraulic fractures. The closer the distance from the hydraulic fractures, the smaller the size and thus the easier the fluid flow. On the contrary, the further the distance from the hydraulic fractures, the larger the size and thus the harder the fluid flow. An ideal physical model in fractured unconventional reservoir is shown in Fig. 1.

Obviously, the maximum density of microfractures is created close to the macrofractures, interpretated as the large amount of minimal matrix block with high matrix−fracture contact area, which also represents the real reservoir condition. For the fluid flow in unconventional reservoir, the well performance depends on the transfer of fluids from tight matrix block to the fracture networks. Because of the ultra-tight permeability, the main flow pattern is considered to be the transient linear flow from matrix block to fractures. In addition, the transient linear flow is affected by the matrix block distribution and matrix−macrofracture communication, which is analyzed in the following section.

2.2. Matrix block distribution

For the continuous distribution of matrix block, the probability density function can be adopted to define the distribution (Al-Rbeawi, 2018).
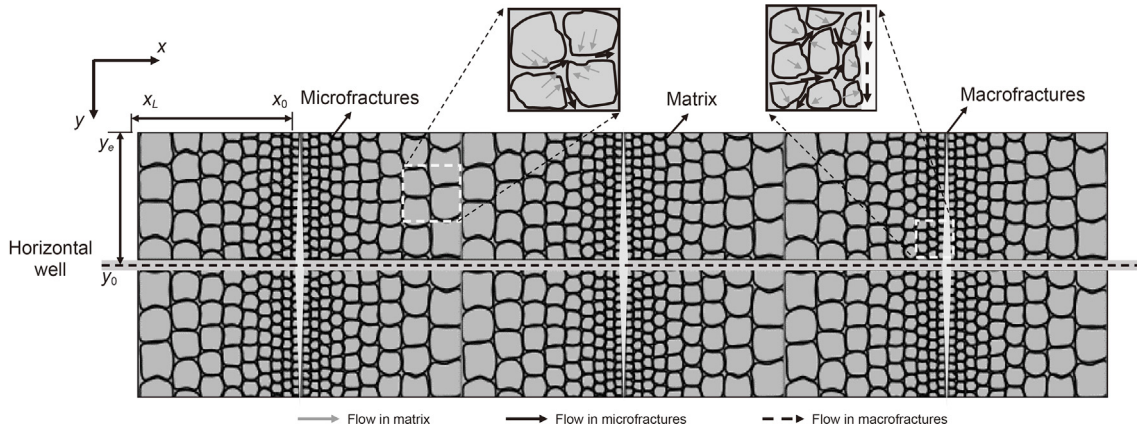
Fig. 1. Conceptual model of multi-stage fractured horizontal well in tight reservoirs with variable matrix block sizes.

$$\int_{L_{\min}}^{L_{\max}} f(L)\mathrm{d}L = 1. \tag{1}$$

In regard of the distance-independency matrix block distribution, a simplest matrix block distribution has been represented mathematically by linear functions (Segall, 1981). The probability density function for linear and exponential distribution can be written in dimensionless form. Among them, two parameters m and b represent the slope and intercept, respectively, which was proposed and defined by Rafael et al. (2002). As for the value of m, positive value indicates the large matrix block and negative value indicates the small matrix block.

$$f(L) = mL + b. \tag{2}$$

2.3. Simultaneous matrix depletion

Some microseismic results have indicated that the stimulated reservoir volume (SRV) including complex fracture networks will be created around the macrofractures after fracturing. In these regions, the ultra-low permeability matrix is broken into smaller pieces and high density of microfractures could be activated because of the high injection pressure. Therefore, the matrix−macrofractures communication could be active (Fig. 1) and the simultaneous matrix depletion must be taken into consideration to avoid unreasonable estimation of the production. Based on the distribution of matrix block, the size of matrix blocks will be larger when moving outward the microfracture. In these situations, there is negligible matrix−macrofracture contact area compared to matrix−microfracture contact area and the flow occurs between the larger-sized matrix blocks and microfractures (Fig. 1). Based on the previous works (Ezulike and Dehghanpour, 2014; Qiu and Li, 2019), the simultaneous matrix depletion, which represents the 2-D linear flow process in the matrix, is divided into two 1-D linear flow processes in order to simplify the derivation, as shown in Fig. 2. As an extension of the previous work, we focus on the derivation of approximate analytical solution considering the distance-dependent matrix blocks in this paper.

2.4. Model development

According to the above section, the matrix is divided into two submatrix to describe two 1-D linear flow processes. Among them,

submatrix m1 (the darker matrix part) feeds the macrofractures in the x direction, and submatrix m2 feeds the microfractures in the y direction. The whole derivation process begins with writing a series of partial differential equations describing the fluid flow in each medium. First, the flow process within submatrix m1 can be expressed as

$$\frac{\partial^2 p_{\mathrm{m1}}}{\partial x^2} + \frac{\partial^2 p_{\mathrm{m1}}}{\partial y^2} + \frac{\partial^2 p_{\mathrm{m1}}}{\partial z^2} = \frac{(\phi\mu c_{\mathrm{t}})_{\mathrm{m1}}}{k_{\mathrm{m1}}} \frac{\partial p_{\mathrm{m1}}}{\partial t} + \frac{\mu_{\mathrm{m1}}}{k_{\mathrm{m1}}} \int_0^L q_{\mathrm{m1\_Ma}} f(L)\mathrm{d}L, \tag{3}$$

$$p_{\mathrm{m1}}(x, y, z, 0) = p_{\mathrm{i}}, \tag{4}$$

$$\frac{k_{\mathrm{F}}}{\mu_{\mathrm{F}}} \left.\frac{\partial p_{\mathrm{F}}}{\partial x}\right|_{x=x_1} = \frac{k_{\mathrm{m1}}}{\mu_{\mathrm{m1}}} \left.\frac{\partial p_{\mathrm{m1}}}{\partial x}\right|_{x=x_1}, \tag{5}$$

$$\left.\frac{\partial p_{\mathrm{m1}}}{\partial x}\right|_{x=x_L} = 0, \tag{6}$$

$$\left.\frac{\partial p_{\mathrm{m1}}}{\partial y}\right|_{y=y_m} = 0, \tag{7}$$

$$\left.\frac{\partial p_{\mathrm{m1}}}{\partial y}\right|_{y=y_e} = 0, \tag{8}$$

$$\left.\frac{\partial p_{\mathrm{m1}}}{\partial z}\right|_{z=z_0} = 0, \tag{9}$$

$$\left.\frac{\partial p_{\mathrm{m1}}}{\partial z}\right|_{z=z_e} = 0, \tag{10}$$

where $q_{\mathrm{m1\_Ma}}$ is the interporosity-flow between submatrix m1 and macrofractures.

Eq. (4) represents the initial constant-pressure conditions. Eq. (5) indicates that the flow rate is equal at the interface between submatrix m1 and the macrofractures. Eqs. (6)–(10) indicate no-flow outer boundary conditions.

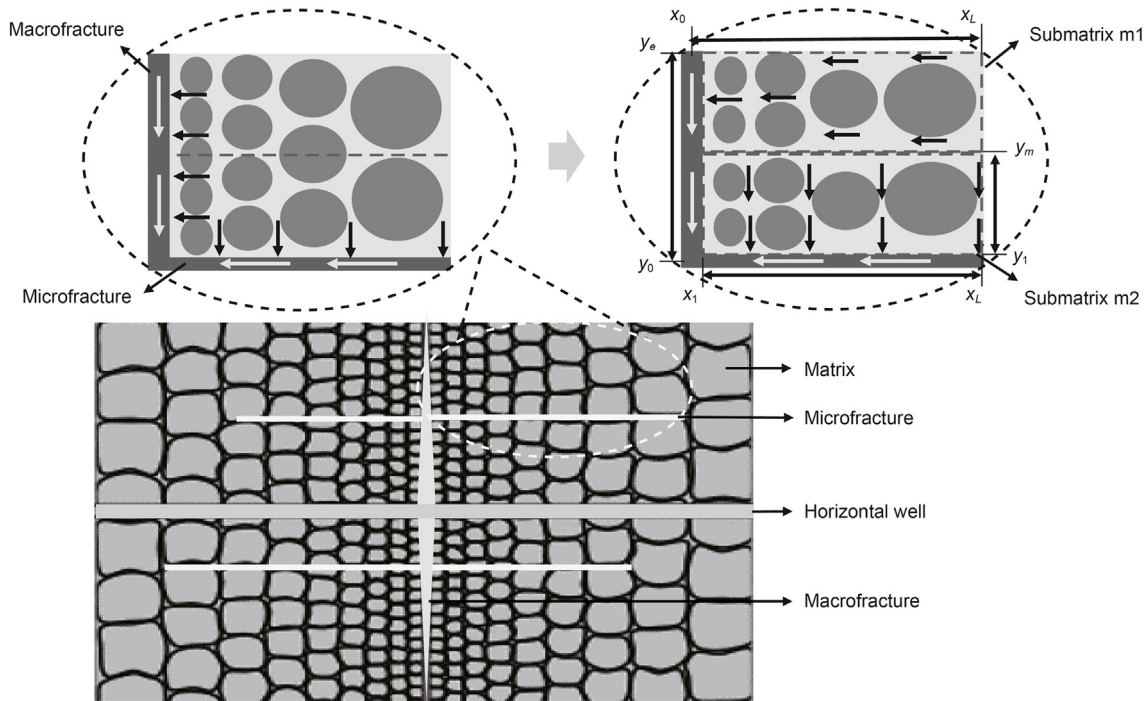Similarly, the expression for transient linear flow within submatrix m2 is

Fig. 2. Conceptual flow model of simultaneous matrix depletion.

$$\frac{\partial^2 p_{m2}}{\partial x^2} + \frac{\partial^2 p_{m2}}{\partial y^2} + \frac{\partial^2 p_{m2}}{\partial z^2} = \frac{(\phi\mu c_t)_{m2}}{k_{m2}} \frac{\partial p_{m2}}{\partial t} + \frac{\mu_{m2}}{k_{m2}} \int_0^L q_{m2\_Mi} f(L) dL,$$

$$(11)$$

$$p_{m2}(x, y, z, 0) = p_i, \tag{12}$$

$$\frac{k_f}{\mu_f} \frac{\partial p_f}{\partial y}\bigg|_{y=y_1} = \frac{k_{m2}}{\mu_{m2}} \frac{\partial p_{m2}}{\partial y}\bigg|_{y=y_1}, \tag{13}$$

$$\frac{\partial p_{m2}}{\partial x}\bigg|_{x=x_1} = 0, \tag{14}$$

$$\frac{\partial p_{m2}}{\partial x}\bigg|_{x=x_L} = 0, \tag{15}$$

$$\frac{\partial p_{m2}}{\partial y}\bigg|_{y=y_m} = 0, \tag{16}$$

$$\frac{\partial p_{m2}}{\partial z}\bigg|_{z=z_0} = 0, \tag{17}$$

$$\frac{\partial p_{m2}}{\partial z}\bigg|_{z=z_e} = 0, \tag{18}$$

where q_{m2_Mi} is the interporosity-flow between submatrix m2 and microfractures. Eq. (12) indicates that the initial pressure is constant. Eq. (13) indicates that the flow rate is equal at the interface between submatrix m2 and the microfractures. Eqs. (14)–(19) represent no-flow outer boundary conditions.

In regard to the microfractures, the flow process is in the x

direction. Therefore, the following mathematical expressions including initial condition and boundary conditions apply

$$\frac{\partial^2 p_f}{\partial x^2} + \frac{\partial^2 p_f}{\partial y^2} + \frac{\partial^2 p_f}{\partial z^2} = \frac{(\phi\mu c_t)_f}{k_f} \frac{\partial p_f}{\partial t}, \tag{19}$$

$$p_f(x, y, z, 0) = p_i, \tag{20}$$

$$\frac{k_f}{\mu_f} \frac{\partial p_f}{\partial y}\bigg|_{y=y_1} = \frac{k_{m2}}{\mu_{m2}} \frac{\partial p_{m2}}{\partial y}\bigg|_{y=y_1}, \tag{21}$$

$$\frac{k_f}{\mu_f} \frac{\partial p_f}{\partial x}\bigg|_{x=x_1} = \frac{k_F}{\mu_F} \frac{\partial p_F}{\partial x}\bigg|_{x=x_1}, \tag{22}$$

$$\frac{\partial p_f}{\partial x}\bigg|_{x=x_L} = 0, \tag{23}$$

$$\frac{\partial p_f}{\partial y}\bigg|_{y=0} = 0, \tag{24}$$

$$\frac{\partial p_f}{\partial z}\bigg|_{z=z_0} = 0, \tag{25}$$

$$\frac{\partial p_f}{\partial z}\bigg|_{z=z_e} = 0. \tag{26}$$

Eq. (20) indicates the initial pressure is constant inside the microfractures. Eq. (21) represents the equal flow rate at the location of $y = y_1$ between submatrix m2 and the microfractures. Similarly, the equal rate between the micro- and macrofractures occurs at the location of $x = x_1$, as expressed in Eq. (22). Eqs. (23)–(26) represent no-flow outer boundary conditions.

Fluid flow inside macrofractures towards the wellbore is in the y direction. The following mathematical expressions including initial condition and boundary conditions apply

$$\frac{\partial^2 p_F}{\partial x^2} + \frac{\partial^2 p_F}{\partial y^2} + \frac{\partial^2 p_F}{\partial z^2} = \frac{(\phi \mu c_t)_F}{k_F} \frac{\partial p_F}{\partial t}, \tag{27}$$

$$p_F(x, y, z, 0) = p_i, \tag{28}$$

$$p_F(x, y_0, z, 0) = p_{wf}, \tag{29}$$

$$\frac{k_F}{\mu_F} \frac{\partial p_F}{\partial x}\bigg|_{x=x_1} = \frac{k_{m1}}{\mu_{m1}} \frac{\partial p_{m1}}{\partial x}\bigg|_{x=x_1}, \tag{30}$$

$$\frac{k_F}{\mu_F} \frac{\partial p_F}{\partial x}\bigg|_{x=x_1} = \frac{k_f}{\mu_f} \frac{\partial p_f}{\partial x}\bigg|_{x=x_1}, \tag{31}$$

$$\frac{\partial p_F}{\partial x}\bigg|_{x=0} = 0, \tag{32}$$

$$\frac{\partial p_F}{\partial y}\bigg|_{y=y_e} = 0, \tag{33}$$

$$\frac{\partial p_F}{\partial z}\bigg|_{z=z_0} = 0, \tag{34}$$

$$\frac{\partial p_F}{\partial z}\bigg|_{z=z_e} = 0. \tag{35}$$

Eq. (28) indicates the initial pressure is constant inside the macrofractures, while Eq. (29) reflects the assumption of a constant bottom-hole pressure (BHP). Eq. (30) represents the principle of fluid continuity between submatrix m1 and the macrofractures at the location of $x = x_1$. Eq. (31) is identical to Eq. (22). Eqs. (32)–(35) represent no-flow outer boundary conditions.

2.5. Solution methodology

In this paper, the integration method is adopted to solve the series of partial differential equations. Moreover, the average pressure in the different media is defined as the volume weighted average, and we can thus transform the above system of partial differential equations (PDEs) into a system of ordinary differential equations (ODEs). A detailed derivation has been provided in

Appendix A. The series of ODEs is obtained as follows:

$$-C_1 q_{m1\_Ma} = (V_p c_t)_{m1} \frac{d\overline{p_{m1}}}{dt}, \tag{36}$$

$$-C_2 q_{m2\_Mi} = (V_p c_t)_{m2} \frac{d\overline{p_{m2}}}{dt}, \tag{37}$$

$$-q_f + q_{m2\_Mi} = (V_p c_t)_f \frac{d\overline{p_f}}{dt}, \tag{38}$$

$$-q_F + q_f + q_{m1\_Ma} = (V_p c_t)_F \frac{d\overline{p_F}}{dt}. \tag{39}$$

As for the above equations, it is necessary to eliminate the average pressure in the next step. Based on the analytical solution for transient linear flow under constant pressure condition (Wattenbarger et al., 1998; Ogunyomi et al., 2016), the average pressure in the different media can be written as

$$\overline{p_F} = p_{wf} + \frac{q_{Fi}}{J_F} \sum_{n=1}^{\infty} \frac{q_{DFn}}{(2n-1)^2}, \tag{40}$$

$$\overline{p_f} = \overline{p_F} + \frac{q_{fi}}{T_{Ff}} \sum_{n=1}^{\infty} \frac{q_{Dfn}}{(2n-1)^2}, \tag{41}$$

$$\overline{p_{m2}} = \overline{p_f} + \frac{q_{im2\_Mi}}{T_{fm2}} \sum_{n=1}^{\infty} \frac{q_{Dm2n}}{(2n-1)^2}, \tag{42}$$

$$\overline{p_{m1}} = \overline{p_F} + \frac{q_{im1\_Ma}}{T_{fm1}} \sum_{n=1}^{\infty} \frac{q_{Dm1n}}{(2n-1)^2}. \tag{43}$$

Substituting Eqs. (40)–(43) into Eqs. (36)–(39) and then rewriting the above ODEs in the following matrix form:

$$\begin{bmatrix} \dfrac{dq_{nm1\_Ma}}{dt} \\[2ex] \dfrac{dq_{nm2\_Mi}}{dt} \\[2ex] \dfrac{dq_{fn}}{dt} \\[2ex] \dfrac{dq_{Fn}}{dt} \end{bmatrix} = (2n-1)^2 \begin{bmatrix} 0 & -\left(\dfrac{1}{\tau_{m1}} + \dfrac{T_{Fm1}}{\tau_F J_F}\right) & -\dfrac{T_{Fm1}}{\tau_F J_F} & \dfrac{T_{Fm1}}{\tau_F J_F} \\[2ex] -\left(\dfrac{1}{\tau_{m2}} + \dfrac{T_{fm2}}{\tau_f T_{Ff}}\right) & 0 & \dfrac{T_{fm2}}{\tau_f T_{Ff}} & 0 \\[2ex] \dfrac{1}{\tau_F} & -\dfrac{T_{Ff}}{\tau_F J_F} & -\left(\dfrac{1}{\tau_f} + \dfrac{T_{Ff}}{\tau_F J_F}\right) & \dfrac{T_{Ff}}{\tau_F J_F} \\[2ex] 0 & \dfrac{1}{\tau_F} & \dfrac{1}{\tau_F} & -\dfrac{1}{\tau_F} \end{bmatrix} \begin{bmatrix} C_1 q_{nm1\_Ma} \\ C_2 q_{nm2\_Mi} \\ q_{fn} \\ q_{Fn} \end{bmatrix}, \tag{44}$$

where the parameters are defined as

$$J_F = \frac{\pi^2}{4} \frac{q_{Fi}}{p_i - p_{wf}},$$

$$T_{Ff} = \frac{\pi^2}{4} \frac{q_{fi}}{\overline{p_f} - \overline{p_F}},$$

$$T_{Fm1} = \frac{\pi^2}{4} \frac{q_{im1\_Ma}}{\overline{p_{m1}} - \overline{p_F}},$$

$$T_{fm2} = \frac{\pi^2}{4} \frac{q_{im2\_Mi}}{\overline{p_{m2}} - \overline{p_f}},$$

$$\tau_F = \frac{(V_p c_t)_F}{J_F},$$

$$\tau_f = \frac{(V_p c_t)_f}{T_{Ff}},$$

$$\tau_{m1} = \frac{(V_p c_t)_{m1}}{T_{Fm1}},$$

$$\tau_{m2} = \frac{(V_p c_t)_{m2}}{T_{fm2}}.$$

$$q_{Fi} = \frac{k_F A_F}{\mu x_F}\left(p_i - p_{wf}\right),$$

$$q_{fi} = \frac{k_f A_f}{\mu x_f}\left(\overline{p_f} - \overline{p_F}\right),$$

$$q_{m1i} = \frac{k_{m1} A_{m1}}{\mu x_{m1}}(\overline{p_{m1}} - \overline{p_F}),$$

$$q_{m2i} = \frac{k_{m2} A_{m2}}{\mu x_{m2}}\left(\overline{p_{m2}} - \overline{p_f}\right).$$

After a series of mathematical manipulations (details in Appendix B), the analytical solution presenting directly oil rate versus production time can be derived. In Eq. (45), λ_1, λ_2, λ_3, λ_4 and ξ_1, ξ_2, ξ_3, ξ_4 are four eigenvalues and four eigenvectors of parameter matrix in Eq. (44) and r_1-r_{16} represent the elements in eigenvectors.

$$
\begin{aligned}
q_F = {} & \beta_1\beta_3 r_4 q_{Fin}e^{\lambda_1 t} + \beta_1\beta_2 r_8 q_{Fin}e^{\lambda_2 t} - \beta_1\alpha_4 r_{12}q_{Fin}e^{\lambda_3 t} \\
& + \beta_1\alpha_3 r_{16}q_{Fin}e^{\lambda_4 t} + \frac{\sqrt{\pi}\beta_1\beta_3 r_4 q_{Fin}}{4\sqrt{|\lambda_1|t}}\,\mathrm{erfc}\left(3\sqrt{|\lambda_1|t}\right) \\
& + \frac{\sqrt{\pi}\beta_1\beta_2 r_8 q_{Fin}}{4\sqrt{|\lambda_2|t}}\,\mathrm{erfc}\left(3\sqrt{|\lambda_2|t}\right) \\
& - \frac{\sqrt{\pi}\beta_1\alpha_4 r_{12}q_{Fin}}{4\sqrt{|\lambda_3|t}}\,\mathrm{erfc}\left(3\sqrt{|\lambda_3|t}\right) \\
& + \frac{\sqrt{\pi}\beta_1\alpha_3 r_{16}q_{Fin}}{4\sqrt{|\lambda_4|t}}\,\mathrm{erfc}\left(3\sqrt{|\lambda_4|t}\right).
\end{aligned}
\tag{45}
$$

where the coefficients in the analytical solution are defined as

$$\alpha_1 = (r_1 r_{12} - r_4 r_9)(r_1 r_6 - r_2 r_5) - (r_1 r_{10} - r_2 r_9)(r_1 r_8 - r_4 r_5),$$

$$\alpha_2 = (r_1 r_{16} - r_4 r_{13})(r_1 r_6 - r_2 r_5) - (r_1 r_{14} - r_2 r_{13})(r_1 r_8 - r_4 r_5),$$

$$\alpha_3 = (r_1 r_{11} - r_3 r_9)(r_1 r_6 - r_2 r_5) - (r_1 r_{10} - r_2 r_9)(r_1 r_7 - r_3 r_5),$$

$$\alpha_4 = (r_1 r_{15} - r_3 r_{13})(r_1 r_6 - r_2 r_5) - (r_1 r_{14} - r_2 r_{13})(r_1 r_7 - r_3 r_5),$$

$$\beta_1 = \frac{r_1(r_1 r_6 - r_2 r_5)}{\alpha_2\alpha_3 - \alpha_1\alpha_4},$$

$$\beta_2 = \frac{\alpha_4(r_1 r_{11} - r_3 r_9) - \alpha_3(r_1 r_{15} - r_3 r_{13})}{r_1 r_7 - r_3 r_5},$$

$$\beta_3 = \frac{\alpha_4 r_9 - \alpha_3 r_{13} - \beta_2 r_5}{r_1}.$$

Obviously, we can find that the oil rate is related to nine variables in Eq. (45), i.e., the time constants of the macrofractures, microfractures and submatrices m1 and m2, productivity index and three transmissibility values. Moreover, the initial production rate of the macrofractures is also important in the analytical solution. The variables in Eq. (45) can be obtained by fitting and are substituted into the solution for further production prediction.

3. Model validation

Validation against the Laplace-transform solution. In this section, we compare the proposed analytical solution to typical Laplace-transform solutions. Firstly, the triple-porosity model proposed by Samandarli (2012) is chosen to obtain convincing results. Because it is not only a classical and reliable model, but also has nearly identical model assumptions and boundary conditions to the new model in this paper. Obviously, the result of new model matches perfectly with Samandarli's analytical solution in Fig. 3(a). Therefore, it is concluded that our model is applicable in triple-porosity reservoirs.

Moreover, the Laplace-transform solution derived by Ezulike and Dehghanpour (2014) is also chosen for verification. The main reason is the authors proposed a quadrilinear flow model (QFM) considering simultaneous matrix−microfracture and matrix−macrofracture depletion. Before verifying the results, their solution has to be numerically inverted through Stehfest (1970) algorithms. It is evident that our model also matches their analytical solution very well in Fig. 3(b). Furthermore, four main flow regimes are identified. Regimes 1 and 3 have both the linear slope of $-1/2$ and represent the transient linear flow in microfracture and transient linear flow from matrix to microfracture, respectively. Regime 4 exhibits the exponential flow decline which means the no-flow boundaries have been reached. Comparing Fig. 3(a) and (b), regime 2 with the slope of $-1/4$ is special and can be interpreted as bilinear flow due to simultaneous linear flow in macrofracture and microfracture. In most cases, regime 3 is regarded as the target regime for fitting production data in the field because the matrix in unconventional reservoirs contributes significantly to production.

Verification against numerical model. Based on the symmetry assumption, a numerical model which is represented simply with three interacting media (matrix, two microfractures and one macrofracture) has been constructed, whose top view is shown in Fig. 4. Meanwhile, the local grid refinement is implemented to 41 grids in the x direction and 49 grids in the y direction in order to describe the variable matrix block sizes. The pressure profile also represents the variable matrix blocks and simultaneous matrix depletion. Table 1 summarizes the important parameters used in numerical model.

In general, the oil rate obtained from the numerical model (black circle) and the new model (red line) suitably agree with each other, as illustrated in Fig. 5. Table 2 summarizes the output parameters from our model after fitting. Obviously, three flow regimes could be identified. The time constant for transient linear flow in macro-fracture is 0.005 d and thus regime 1 is too short to be observed.
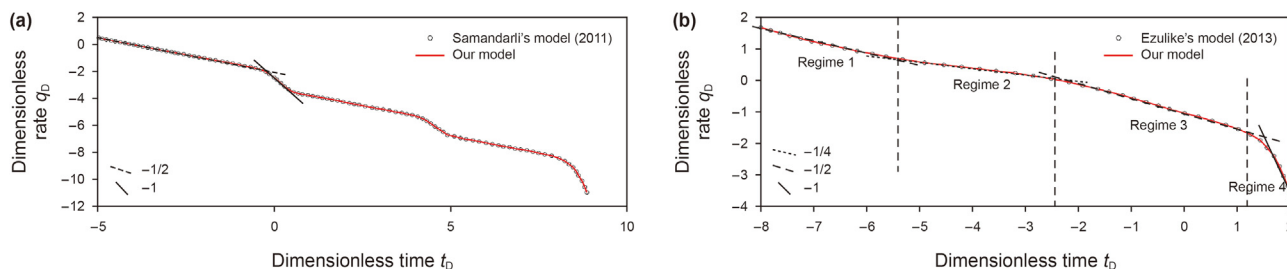
Fig. 3. (**a**) Comparison of our model with the triple-porosity Laplace-transform solution; (**b**) Comparison of our model with Laplace-transform solution considering the simultaneous matrix depletion.
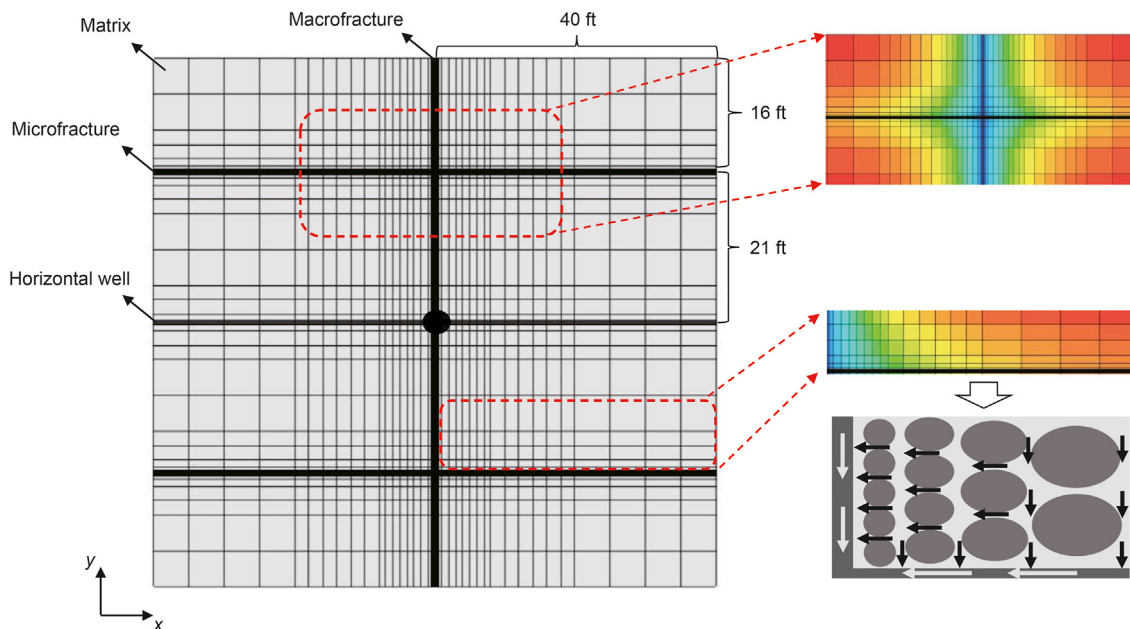

Fig. 4. Top view of the numerical model.

Table 1
Basic parameters for numerical case.

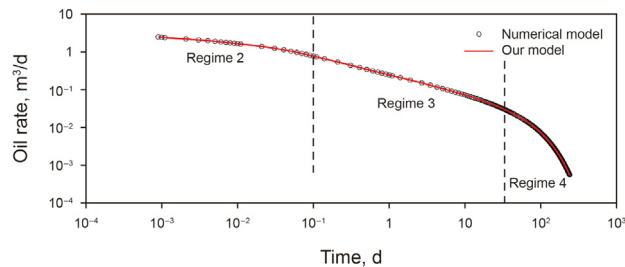| Parameters	Value
Model dimensions ($x \times y \times z$), ft	$80 \times 74 \times 3$
Initial pressure, psi	2500
Bottom-hole pressure, psi	500
Viscosity, cP	3
Oil compressibility, 10^{-5} psi^{-1}	9.75
Rock compressibility, 10^{-6} psi^{-1}	6.1
Porosity	0.06
Macrofracture permeability, mD	50
Microfracture permeability, mD	5
Matrix permeability, mD	0.001
Volume of macrofractures, ft^3	22.2
Volume of microfractures, ft^3	4.8
Volume of the matrix, ft^3	17733

Fig. 5. Comparison verification between the numerical case and new model.

Table 2
Output parameters after validating against the numerical model.

Parameter	Value
τ_{m1}, d	55
τ_{m2}, d	85
τ_f, d	0.08
τ_F, d	0.005
T_{fm1}/T_{Ff}	0.108
T_{Fm2}/J_F	0.08
T_{Ff}/J_F	0.143
q_{Fi}, STB/d	1.24

The microfracture time constants are 0.08 d and regime 2 can last about 0.1 d. Regime 3 represents transient linear flow from submatrix m2 to microfracture and can be observed to last for 85 d. The no-flow boundaries can be reached when the production time is long enough and then regime 4 can also be observed.
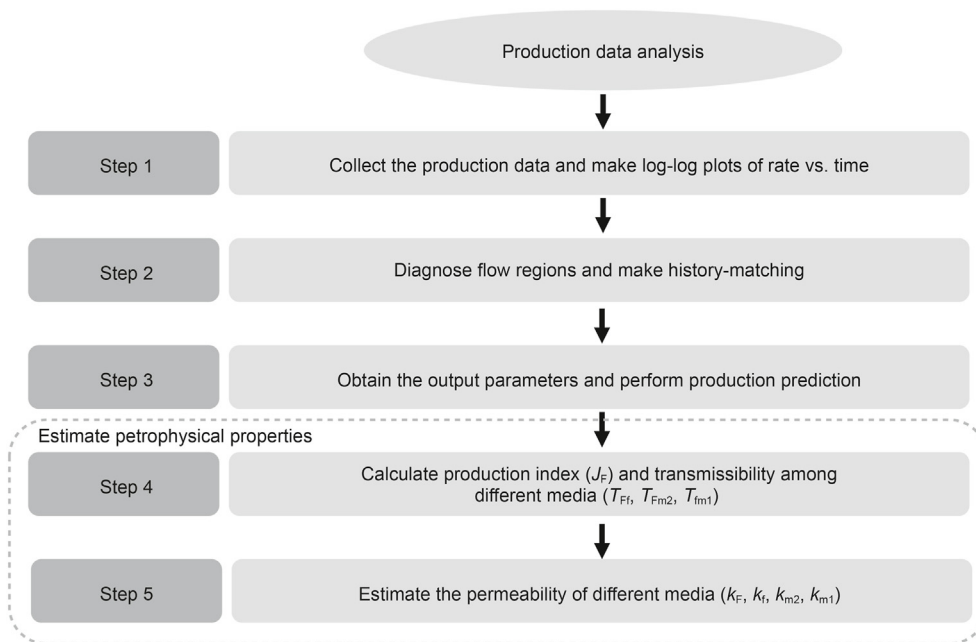
Fig. 6. Flowchart for production data analysis.

4. Production data analysis and field application

4.1. Production data analysis

The accuracy of the new model has been validated by comparing with typical analytical solutions and numerical model. In this section, a flow chart is developed for applying the new model to field data to make production analysis easier, which is presented in Fig. 6. The first three steps focus on the data processing and history matching. The main purpose is to get the output parameters of the new model through fitting. The obtained parameters are not only substituted into the new model for production prediction, but also can be used to estimate the petrophysical properties because they strictly follow the mathematical and physical definition according to the last two steps.

4.2. Field application

Example 1. CARD-1 is a horizontal well with 10 stages of hydro-fracturing stimulation which is drilled to exploit the Halo oil play in western Canada sedimentary basin. This well has been on constant bottom-hole pressure production for just over 400 d and the production data can be retrieved from Clarkson and Pedersen (2011).

Table 3
Output parameter values after fitting.

Parameter	CARD-1	2WS-1
τ_{m1}, d	133	238
τ_{m2}, d	248	2488
τ_{f}, d	0.03	229
τ_{F}, d	0.001	0.002
T_{fm1}/T_{Ff}	0.33	0.3
T_{Fm2}/J_{F}	0.65	0.75
T_{Ff}/J_{F}	0.15	0.14
q_{Fi}, STB/d	367	686

Table 4
Estimated parameter values according to the production data analysis.

Parameter	CARD-1	2WS-1
V_{m1}, 10^5 m^3	4.4	69.7
V_{m2}, 10^5 m^3	38.7	118.7
V_{f}, m^3	35	4322
V_{F}, m^3	17	61
K_{m1}, mD	0.001	0.0006
K_{m2}, mD	0.003	0.0002
K_{f}, mD	3	4
K_{F}, mD	150	30

Fig. 7. The application of the new model in well CARD-1. (**a**) Actual oil rate in log-log plot; (**b**) Results by history matching and forecasting in log-log plot.
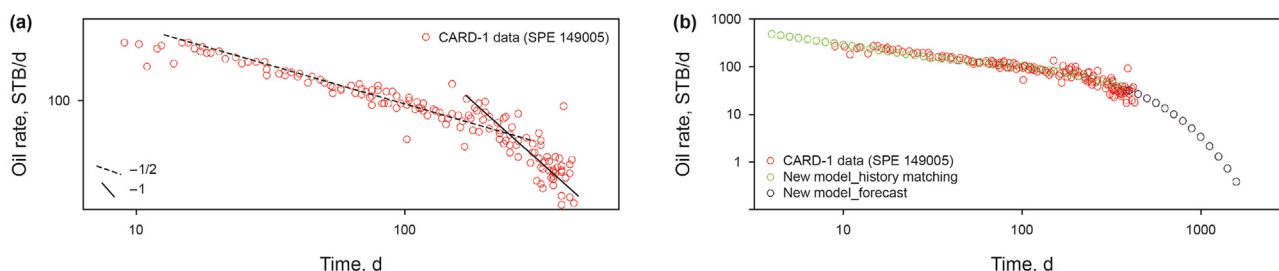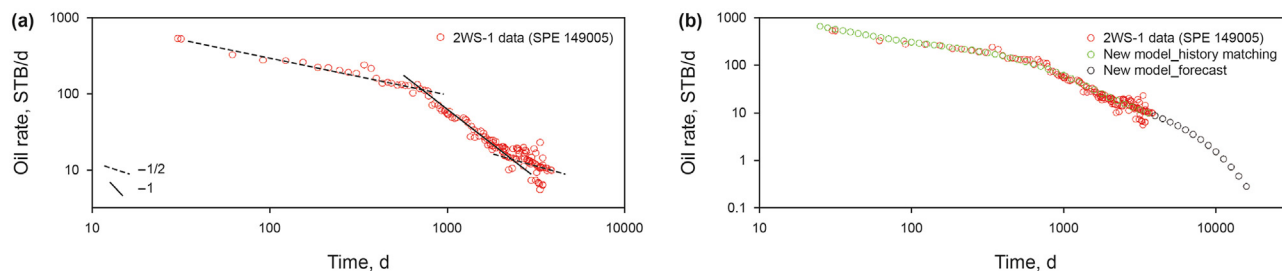
Fig. 8. The application of the new model in well 2WS-1. (**a**) Actual oil rate in log-log plot; (**b**) Results by history matching and forecasting in log-log plot.

The half-slope and unit-slope on the log-log plot can be exhibited in Fig. 7(a) and is essential for diagnosing the dominant flow regimes. The first flow period lasts over 200 d, and the second flow period represents that the pressure reaches the boundaries. Therefore, the two flow regimes in Fig. 7(a) can be diagnosed separately as regime 3 and regime 4. According to the flowchart, the new model is then used for matching the actual data and forecasting the future production. The fitting and prediction results are shown in Fig. 7(b). The fitting results indicate a good matching, and all output and estimated parameters are listed in Tables 3 and 4, respectively. Obviously, the macro- and microfracture time constants are determined as 0.001 and 0.03 d respectively. Thus, regime 1 and regime 2 are too short to be observed. The feed times for submatrices 1 and 2 are estimated to be 133 and 248 d. In other words, the transient linear flow from matrix to macrofracture accounts for almost half of the matrix transient flow time, which is also an important proof to considering simultaneous matrix depletion.

Example 2. Well 2WS-1 is a typical vertical shale oil well which was used to develop the Second White Speckled Shale in Canada. This well was in continuous production under constant bottom-hole pressure for approximately 3500 d. Similarly, the production data is extracted from Clarkson and Pedersen (2011) and exhibited on the log-log diagnostic plot which is shown in Fig. 8(a). Three flow regimes could be identified including two transient linear flow and one early unit-slope. Considering the first linear flow period lasted for longer than 600 d and the second linear flow period lasted approximately 2000 d, the second half-slope linear flow can be diagnosed as regime 3. The next step involves history matching the production data with our new model. The excellent fitting and prediction results can be obtained and shown in Fig. 8(b). All output and estimated parameters are listed in Tables 3 and 4, respectively. According to the output parameters, the feed times for submatrix m1 is much lower than that of submatrix m2. It is likely that the permeability of macrofracture is closer to that of microfractures.

5. Conclusions

In this study, we developed an approximately analytical solution to account for the variable matrix blocks and simultaneous matrix depletion in unconventional oil reservoirs. In addition to make production prediction, the solution can be used to capture the flow contribution from non-uniformly distributed matrix and then interpret the field data. The specific conclusions can be summarized.

(1) During the mathematical derivation, the partial-differential equations (PDEs) constructing mathematical models are transformed into ordinary-differential equations (ODEs) by integration and average pressure replacement. A rate-vs.-time solution in real-time space can be obtained, bypassing the numerical inversion for the Laplace transform. The linear flow regions are easy to be diagnosed and the corresponding flow time can be obtained directly after fitting which is convenient for reservoir and engineering application.

(2) The analytical model provides a practical approach to consider simultaneous matrix–macrofracture and matrix–microfracture depletion by breaking a single 2-D problem into two 1-D problems. A typical flow region (a quarter-slope) can be observed because of the significant matrix–macrofracture communication, which will help for reasonable estimation of microfracture and/or macrofracture properties. Comparing with the existing dual- and triple-porosity models, the proposed model is more comprehensive.

(3) In contrast to the existed models that consider the fixed matrix-block size, the distribution of the matrix blocks depends on the distance from the main hydraulic-fracture plane which is expressed mathematically by typical linear functions in the paper. After fracturing, a high density of microfractures is created near macrofractures. Namely, the smaller matrix block near macrofractures with higher matrix–macrofracture contact area could enhance the transfer of fluids from matrix to macrofractures and have a positive impact on well performance.

(4) The parameters in the analytical solution are defined strictly following the mathematical and physical meanings. Especially for time constants, they are strongly correlated with the porous volume of each medium. Based on the output parameters, the porous volume and permeability of each medium can be inferred, which is significant for well test and production prediction.

Declaration of interest

The authors declare that they have no known competing financial interests or personal relationships that could have appeared to influence the work reported in this paper.

Acknowledgments

Appendix A

In regard to the governing equation of submatrix m1 expressed as Eq. (3), multiple integrals are computed with x ranging from x_1 to x_L, y ranging from y_m to y_e and z ranging from z_0 to z_e:

$$\int_{x_1}^{x_L} \int_{y_m}^{y_e} \int_{z_0}^{z_e} \left(\frac{\partial^2 p_{m1}}{\partial x^2} + \frac{\partial^2 p_{m1}}{\partial y^2} + \frac{\partial^2 p_{m1}}{\partial z^2} \right) \mathrm{d}x\mathrm{d}y\mathrm{d}z$$

$$= \frac{(\phi\mu c_t)_{m1}}{k_{m1}} \int_{x_1}^{x_L} \int_{y_m}^{y_e} \int_{z_0}^{z_e} \left(\frac{\partial p_{m1}}{\partial t} \right) \mathrm{d}x\mathrm{d}y\mathrm{d}z$$

$$+ \int_{x_1}^{x_L} \int_{y_m}^{y_e} \int_{z_0}^{z_e} \left(\frac{\mu_{m1}}{k_{m1}} \int_0^L q_{m1\_Ma} f(L)\mathrm{d}L \right) \mathrm{d}x\mathrm{d}y\mathrm{d}z. \tag{A1}$$

Removing space-independent time t outside of the spatial integral gives

$$\int_{x_1}^{x_L} \int_{y_m}^{y_e} \int_{z_0}^{z_e} \frac{\partial}{\partial x} \left(\frac{\partial p_{m1}}{\partial x} \right) \mathrm{d}x\mathrm{d}y\mathrm{d}z + \int_{x_1}^{x_L} \int_{y_m}^{y_e} \int_{z_0}^{z_e} \frac{\partial}{\partial y} \left(\frac{\partial p_{m1}}{\partial y} \right) \mathrm{d}x\mathrm{d}y\mathrm{d}z + \int_{x_1}^{x_L} \int_{y_m}^{y_e} \int_{z_0}^{z_e} \frac{\partial}{\partial z} \left(\frac{\partial p_{m1}}{\partial z} \right) \mathrm{d}x\mathrm{d}y\mathrm{d}z =$$

$$\frac{(\phi\mu c_t)_{m1}}{k_{m1}} \frac{\partial}{\partial t} \int_{x_1}^{x_L} \int_{y_m}^{y_e} \int_{z_0}^{z_e} p_{m1}\mathrm{d}x\mathrm{d}y\mathrm{d}z + \left(\frac{\mu_{m1}}{k_{m1}} q_{m1\_Ma} \int_0^L f(L)\mathrm{d}L \right) \int_{x_1}^{x_L} \int_{y_m}^{y_e} \int_{z_0}^{z_e} \mathrm{d}x\mathrm{d}y\mathrm{d}z. \tag{A2}$$

Firstly, the volume-averaged pressure can be defined as

$$\overline{p} = \frac{\int p\mathrm{d}V}{V}. \tag{A3}$$

Therefore, the average pressure of three interacting media can be expressed sequentially as

$$\overline{p_{m1}} = \frac{\displaystyle\int_{x_1}^{x_L} \int_{y_m}^{y_e} \int_{z_0}^{z_e} p_{m1}\mathrm{d}x\mathrm{d}y\mathrm{d}z}{\displaystyle\int_{x_1}^{x_L} \int_{y_m}^{y_e} \int_{z_0}^{z_e} \mathrm{d}x\mathrm{d}y\mathrm{d}z}, \tag{A4}$$

$$\overline{p_{m2}} = \frac{\displaystyle\int_{x_1}^{x_L} \int_{y_1}^{y_m} \int_{z_0}^{z_e} p_{m2}\mathrm{d}x\mathrm{d}y\mathrm{d}z}{\displaystyle\int_{x_1}^{x_L} \int_{y_1}^{y_m} \int_{z_0}^{z_e} \mathrm{d}x\mathrm{d}y\mathrm{d}z}, \tag{A5}$$

$$\overline{p_f} = \frac{\displaystyle\int_{x_1}^{x_L} \int_0^{y_1} \int_{z_0}^{z_e} p_f\mathrm{d}x\mathrm{d}y\mathrm{d}z}{\displaystyle\int_{x_1}^{x_L} \int_0^{y_1} \int_{z_0}^{z_e} \mathrm{d}x\mathrm{d}y\mathrm{d}z}, \tag{A6}$$

$$\overline{p_F} = \frac{\displaystyle\int_0^{x_1} \int_0^{y_e} \int_{z_0}^{z_e} p_F\mathrm{d}x\mathrm{d}y\mathrm{d}z}{\displaystyle\int_0^{x_1} \int_0^{y_e} \int_{z_0}^{z_e} \mathrm{d}x\mathrm{d}y\mathrm{d}z}. \tag{A7}$$

Similarly, the bulk volume of three interacting media can be defined sequentially as

$$V_{bm1} = \int_{x_1}^{x_L} \int_{y_m}^{y_e} \int_{z_0}^{z_e} \mathrm{d}x\mathrm{d}y\mathrm{d}z, \tag{A8}$$

$$V_{bm2} = \int_{x_1}^{x_L} \int_{y_1}^{y_m} \int_{z_0}^{z_e} \mathrm{d}x\mathrm{d}y\mathrm{d}z, \tag{A9}$$

$$V_{bf} = \int_{x_1}^{x_L} \int_0^{y_1} \int_{z_0}^{z_e} \mathrm{d}x\mathrm{d}y\mathrm{d}z, \tag{A10}$$

$$V_{bF} = \int_0^{x_1} \int_0^{y_e} \int_{z_0}^{z_e} \mathrm{d}x\mathrm{d}y\mathrm{d}z. \tag{A11}$$

Eq. (A4) can be translated into

$$\int_{x_1}^{x_L} \int_{y_1}^{y_e} \int_{z_0}^{z_e} p_{m1}\mathrm{d}x\mathrm{d}y\mathrm{d}z = \overline{p_{m1}} V_{bm1}. \tag{A12}$$

Substituting Eq. (A12) into Eq. (A2), Eq. (A2) can be rewritten as

$$\int_{y_m}^{y_e} \int_{z_0}^{z_e} \left(\frac{\partial p_{m1}}{\partial x}\bigg|_{x_L} - \frac{\partial p_{m1}}{\partial x}\bigg|_{x_1} \right) \mathrm{d}y\mathrm{d}z + \int_{x_1}^{x_L} \int_{z_0}^{z_e} \left(\frac{\partial p_{m1}}{\partial y}\bigg|_{y_e} - \frac{\partial p_{m1}}{\partial y}\bigg|_{y_m} \right) \mathrm{d}x\mathrm{d}z$$

$$+ \int_{x_1}^{x_L} \int_{y_m}^{y_e} \left(\frac{\partial p_{m1}}{\partial z}\bigg|_{z_0} - \frac{\partial p_{m1}}{\partial z}\bigg|_{z_e} \right) \mathrm{d}x\mathrm{d}y$$

$$= \frac{(\phi\mu c_t)_{m1}}{k_{m1}} V_{bm1} \frac{\mathrm{d}\overline{p_{m1}}}{\mathrm{d}t} + \frac{\mu_{m1}}{k_{m1}} V_{bm1} q_{m1\_Ma} \int_0^L f(L)\mathrm{d}L. \tag{A13}$$

Simplifying Eq. (A13) by substituting the boundary conditions, we can obtain

$$-\int_{y_m}^{y_e}\int_{z_0}^{z_e}\left(\frac{k_{m1}}{\mu_{m1}}\frac{\partial p_{m1}}{\partial x}\bigg|_{x_1}\right)dydz = (\phi c_t)_{m1}V_{bm1}\frac{d\overline{p_{m1}}}{dt}$$

$$+ V_{bm1}q_{m1\_Ma}\int_0^L f(L)dL. \quad (A14)$$

According to Darcy's law

$$q_{m1\_Ma} = \int_{y_m}^{y_e}\int_{z_0}^{z_e}\left(\frac{k_{m1}}{\mu_{m1}}\frac{\partial p_{m1}}{\partial x}\bigg|_{x_1}\right)dydz. \quad (A15)$$

Moreover, we define the pore volume of three interacting media as

$$V_{pm1} = V_{bm1}\phi, \quad (A16)$$

$$V_{pm2} = V_{bm2}\phi, \quad (A17)$$

$$V_{pf} = V_{bf}\phi, \quad (A18)$$

$$V_{pF} = V_{bF}\phi. \quad (A19)$$

Eq. (A14) can be rewritten as

$$-C_1 q_{m1\_Ma} = (V_p c_t)_{m1}\frac{d\overline{p_{m1}}}{dt}, \quad (A20)$$

where C_1 is a constant, and $C_1 = 1 + V_{bm1}\int_0^L f(L)dL$.

Similarly, we can obtain the ODE of submatrix m2 as

$$-C_2 q_{m2\_Mi} = (V_p c_t)_{m2}\frac{d\overline{p_{m2}}}{dt}, \quad (A21)$$

where C_2 is a constant, and $C_2 = 1 + V_{bm2}\int_0^L f(L)dL$.

Similarly, the multiple integral transformation is applied to calculating the governing equation of the microfracture:

$$\int_{x_1}^{x_L}\int_0^{y_1}\int_{z_0}^{z_e}\left(\frac{\partial^2 p_f}{\partial x^2} + \frac{\partial^2 p_f}{\partial y^2} + \frac{\partial^2 p_f}{\partial z^2}\right)dxdydz$$

$$= \frac{(\phi\mu c_t)_f}{k_f}\int_{x_1}^{x_L}\int_0^{y_1}\int_{z_0}^{z_e}\left(\frac{\partial p_f}{\partial t}\right)dxdydz. \quad (A22)$$

Eqs. (A6) and (A10) are substituted to simplify Eq. (A22) as

$$\int_0^{y_1}\int_{z_0}^{z_e}\left(\frac{\partial p_f}{\partial x}\bigg|_{x_L} - \frac{\partial p_f}{\partial x}\bigg|_{x_1}\right)dydz + \int_{x_1}^{x_L}\int_{z_0}^{z_e}\left(\frac{\partial p_f}{\partial y}\bigg|_{y_1} - \frac{\partial p_f}{\partial y}\bigg|_0\right)dxdz$$

$$+ \int_{x_1}^{x_L}\int_0^{y_1}\left(\frac{\partial p_f}{\partial z}\bigg|_{z_e} - \frac{\partial p_f}{\partial z}\bigg|_{z_0}\right)dxdy$$

$$= \frac{(\phi\mu c_t)_f}{k_f}V_{bf}\frac{d\overline{p_f}}{dt}. \quad (A23)$$

Multiplying both sides by $\frac{k_f}{\mu_f}$ and simplifying Eq. (A23) based on boundary conditions, we can obtain as

$$-\int_0^{y_1}\int_{z_0}^{z_e}\left(\frac{k_f}{\mu_f}\frac{\partial p_f}{\partial x}\bigg|_{x_1}\right)dydz + \int_{x_1}^{x_L}\int_{z_0}^{z_e}\left(\frac{k_f}{\mu_f}\frac{\partial p_f}{\partial y}\bigg|_{y_1}\right)dxdz = (\phi c_t)_f V_{bf}\frac{d\overline{p_f}}{dt}. \quad (A24)$$

According to Darcy's law

$$q_f = \int_0^{y_1}\int_{z_0}^{z_e}\left(\frac{k_f}{\mu_f}\frac{\partial p_f}{\partial x}\bigg|_{x_1}\right)dydz. \quad (A25)$$

The following flux continuity at the interface between the microfracture and matrix is recognized

$$\frac{k_f}{\mu}\frac{\partial p_f}{\partial y}\bigg|_{y=y_1} = \frac{k_{m2}}{\mu}\frac{\partial p_{m2}}{\partial y}\bigg|_{y=y_1}, \quad (A26)$$

Substituting Eqs. (A25) and (A26) into Eq. (A24), we obtain

$$-q_f + q_{m2\_Mi} = (V_p c_t)_f\frac{d\overline{p_f}}{dt}. \quad (A27)$$

The governing equation of the microfracture can also be calculated by multiple integral transformation:

$$\int_0^{x_1}\int_0^{y_e}\int_{z_0}^{z_e}\left(\frac{\partial^2 p_F}{\partial x^2} + \frac{\partial^2 p_F}{\partial y^2} + \frac{\partial^2 p_F}{\partial z^2}\right)dxdydz$$

$$= \frac{(\phi\mu c_t)_F}{k_F}\int_0^{x_1}\int_0^{y_e}\int_{z_0}^{z_e}\left(\frac{\partial p_F}{\partial t}\right)dxdydz. \quad (A28)$$

Eqs. (A7) and (A11) are substituted to simplify Eq. (A28) and the new expression for Eq. (A28) can be obtained as

$$\int_0^{y_e}\int_{z_0}^{z_e}\left(\frac{\partial p_F}{\partial x}\bigg|_{x_1} - \frac{\partial p_F}{\partial x}\bigg|_0\right)dydz + \int_0^{x_1}\int_{z_0}^{z_e}\left(\frac{\partial p_F}{\partial y}\bigg|_{y_e} - \frac{\partial p_F}{\partial y}\bigg|_0\right)dxdz$$

$$+ \int_0^{x_1}\int_0^{y_e}\left(\frac{\partial p_F}{\partial z}\bigg|_{z_e} - \frac{\partial p_F}{\partial z}\bigg|_{z_0}\right)dxdy$$

$$= \frac{(\phi\mu c_t)_F}{k_F}V_{bF}\frac{d\overline{p_F}}{dt}. \quad (A29)$$

Applying the boundary condition and multiplying both sides by $\frac{k_F}{\mu_F}$, Eq. (A29) can be simplified as

$$\int_0^{y_e}\int_{z_0}^{z_e}\left(\frac{k_F}{\mu_F}\frac{\partial p_F}{\partial x}\bigg|_{x_1}\right)dydz + \int_0^{x_1}\int_{z_0}^{z_e}\left(-\frac{k_F}{\mu_F}\frac{\partial p_F}{\partial y}\bigg|_0\right)dxdz = (V_{pF}c_t)_F\frac{d\overline{p_F}}{dt}. \quad (A30)$$

According to Darcy's law

$$q_F = \int_0^{x_1}\int_{z_0}^{z_e}\left(\frac{k_F}{\mu_F}\frac{\partial p_F}{\partial y}\bigg|_0\right)dxdz. \quad (A31)$$

The following flux continuity at the interface between the micro- and macrofractures is considered

$$\frac{k_{\mathrm{F}}}{\mu_{\mathrm{F}}}\frac{\partial p_{\mathrm{F}}}{\partial x}\bigg|_{x=x_1} = \frac{k_{\mathrm{f}}}{\mu_{\mathrm{f}}}\frac{\partial p_{\mathrm{f}}}{\partial x}\bigg|_{x=x_1},\tag{A32}$$

$$\frac{k_{\mathrm{F}}}{\mu_{\mathrm{F}}}\frac{\partial p_{\mathrm{F}}}{\partial x}\bigg|_{x=x_1} = \frac{k_{\mathrm{m2}}}{\mu_{\mathrm{m2}}}\frac{\partial p_{\mathrm{m2}}}{\partial x}\bigg|_{x=x_1}.\tag{A33}$$

With the microfracture rate expressed in Eq. (A25), Eq. (A30) can be rewritten as

$$-q_{\mathrm{F}} + q_{\mathrm{f}} + q_{\mathrm{m1\_Ma}} = (V_{\mathrm{p}}c_{\mathrm{t}})_{\mathrm{F}}\frac{\mathrm{d}\overline{p_{\mathrm{F}}}}{\mathrm{d}t}.\tag{A34}$$

Appendix B

Substituting Eqs. (40)–(43) into Eqs. (36)–(39), we obtain

$$(V_{\mathrm{p}}c_{\mathrm{t}})_{\mathrm{F}}\left(\frac{q_{\mathrm{Fi}}}{J_{\mathrm{F}}}\sum_{n=1}^{\infty}\frac{1}{(2n-1)^2}\frac{\mathrm{d}q_{\mathrm{DF}n}}{\mathrm{d}t}\right) = -q_{\mathrm{Fi}}\sum_{n=1}^{\infty}q_{\mathrm{DF}n}(t) + q_{\mathrm{fi}}\sum_{n=1}^{\infty}q_{\mathrm{Df}n}(t)$$
$$+ q_{\mathrm{im1.Ma}}\sum_{n=1}^{\infty}q_{\mathrm{D}nm1.Ma}(t),\tag{B1}$$

$$\sum_{n=1}^{\infty}\frac{1}{(2n-1)^2}\frac{\mathrm{d}q_{\mathrm{f}n}}{\mathrm{d}t} = \frac{T_{\mathrm{Ff}}}{(V_{\mathrm{p}}c_{\mathrm{t}})_{\mathrm{f}}}\sum_{n=1}^{\infty}q_{nm1\_Ma}(t) - \frac{T_{\mathrm{Ff}}}{(V_{\mathrm{p}}c_{\mathrm{t}})_{\mathrm{f}}}\sum_{n=1}^{\infty}q_{\mathrm{f}n}(t)$$
$$-\frac{T_{\mathrm{Ff}}}{J_{\mathrm{F}}}\left[-\frac{J_{\mathrm{F}}}{(V_{\mathrm{p}}c_{\mathrm{t}})_{\mathrm{F}}}\sum_{n=1}^{\infty}q_{\mathrm{F}n}(t) + \frac{J_{\mathrm{F}}}{(V_{\mathrm{p}}c_{\mathrm{t}})_{\mathrm{F}}}\sum_{n=1}^{\infty}q_{\mathrm{f}n}(t) + \frac{J_{\mathrm{F}}}{(V_{\mathrm{p}}c_{\mathrm{t}})_{\mathrm{F}}}\sum_{n=1}^{\infty}q_{nm2\_Mi}(t)\right],\tag{B6}$$

$$(V_{\mathrm{p}}c_{\mathrm{t}})_{\mathrm{f}}\left(\frac{q_{\mathrm{Fi}}}{J_{\mathrm{F}}}\sum_{n=1}^{\infty}\frac{1}{(2n-1)^2}\frac{\mathrm{d}q_{\mathrm{DF}n}}{\mathrm{d}t} + \frac{q_{\mathrm{fi}}}{T_{\mathrm{Ff}}}\sum_{n=1}^{\infty}\frac{1}{(2n-1)^2}\frac{\mathrm{d}q_{\mathrm{Df}n}}{\mathrm{d}t}\right)$$
$$= -q_{\mathrm{fi}}\sum_{n=1}^{\infty}q_{\mathrm{Df}n}(t) + q_{\mathrm{im2\_Mi}}\sum_{n=1}^{\infty}q_{\mathrm{D}nm2\_Mi}(t),\tag{B2}$$

$$(V_{\mathrm{p}}c_{\mathrm{t}})_{\mathrm{m2}}\left(\frac{q_{\mathrm{Fi}}}{J_{\mathrm{F}}}\sum_{n=1}^{\infty}\frac{1}{(2n-1)^2}\frac{\mathrm{d}q_{\mathrm{DF}n}}{\mathrm{d}t} + \frac{q_{\mathrm{fi}}}{T_{\mathrm{Ff}}}\sum_{n=1}^{\infty}\frac{1}{(2n-1)^2}\frac{\mathrm{d}q_{\mathrm{Df}n}}{\mathrm{d}t} + \frac{q_{\mathrm{im2\_Mi}}}{T_{\mathrm{fm2}}}\sum_{n=1}^{\infty}\frac{1}{(2n-1)^2}\frac{\mathrm{d}q_{\mathrm{D}nm2\_Mi}}{\mathrm{d}t}\right)$$
$$= -C_2 q_{\mathrm{im2\_Mi}}\sum_{n=1}^{\infty}q_{\mathrm{D}nm2\_Mi}(t),\tag{B3}$$

$$(V_{\mathrm{p}}c_{\mathrm{t}})_{\mathrm{m1}}\left(\frac{q_{\mathrm{Fi}}}{J_{\mathrm{F}}}\sum_{n=1}^{\infty}\frac{1}{(2n-1)^2}\frac{\mathrm{d}q_{\mathrm{DF}n}}{\mathrm{d}t} + \frac{q_{\mathrm{im1.Ma}}}{T_{\mathrm{Fm1}}}\sum_{n=1}^{\infty}\frac{1}{(2n-1)^2}\frac{\mathrm{d}q_{\mathrm{D}nm1.Ma}}{\mathrm{d}t}\right)$$
$$= -q_{\mathrm{im1.Ma}}\sum_{n=1}^{\infty}q_{\mathrm{D}nm1.Ma}(t).\tag{B4}$$

After dividing both sides by certain parameters, the following is obtained

$$\sum_{n=1}^{\infty}\frac{1}{(2n-1)^2}\frac{\mathrm{d}q_{\mathrm{F}n}}{\mathrm{d}t} = -\frac{J_{\mathrm{F}}}{(V_{\mathrm{p}}c_{\mathrm{t}})_{\mathrm{F}}}\sum_{n=1}^{\infty}q_{\mathrm{F}n}(t) + \frac{J_{\mathrm{F}}}{(V_{\mathrm{p}}c_{\mathrm{t}})_{\mathrm{F}}}\sum_{n=1}^{\infty}q_{\mathrm{f}n}(t)$$
$$+ \frac{J_{\mathrm{F}}}{(V_{\mathrm{p}}c_{\mathrm{t}})_{\mathrm{F}}}\sum_{n=1}^{\infty}q_{nm1\_Ma}(t),\tag{B5}$$

$$\sum_{n=1}^{\infty}\frac{1}{(2n-1)^2}\frac{\mathrm{d}q_{nm2\_Mi}}{\mathrm{d}t} = -\left(\frac{T_{\mathrm{fm2}}}{(V_{\mathrm{p}}c_{\mathrm{t}})_{\mathrm{m2}}} + \frac{T_{\mathrm{Ff}}}{(V_{\mathrm{p}}c_{\mathrm{t}})_{\mathrm{f}}}\frac{T_{\mathrm{fm2}}}{T_{\mathrm{Ff}}}\right)C_2\times$$
$$\sum_{n=1}^{\infty}q_{nm2\_Mi}(t) + \frac{T_{\mathrm{Ff}}}{(V_{\mathrm{p}}c_{\mathrm{t}})_{\mathrm{f}}}\frac{T_{\mathrm{fm2}}}{T_{\mathrm{Ff}}}\sum_{n=1}^{\infty}q_{\mathrm{f}n}(t),\tag{B7}$$

$$\sum_{n=1}^{\infty}\frac{1}{(2n-1)^2}\frac{dq_{nm1\_Ma}}{dt} = -\left(\frac{T_{Fm1}}{(V_p c_t)_{m1}}+\frac{J_F}{(V_p c_t)_F}\frac{T_{Fm1}}{J_F}\right)C_1\times$$
$$\sum_{n=1}^{\infty}q_{nm1\_Ma}(t)-\frac{T_{Fm1}}{J_F}\frac{J_F}{(V_p c_t)_F}\sum_{n=1}^{\infty}q_{fn}(t)$$
$$+\frac{T_{Fm1}}{J_F}\frac{J_F}{(V_p c_t)_F}\sum_{n=1}^{\infty}q_{Fn}(t).$$

(B8)

Eqs. (B5)−(B8) can be rewritten in the following matrix form:

$$q_{fn}(t=0)=0,$$

(B13)

$$q_{Fn}(t=0)=q_{Fin}.$$

(B14)

Substituting the initial conditions, Eq. (B9) can be solved analytically to represent the relationship between the production rate and real time.

$$\begin{bmatrix}\dfrac{dq_{nm1\_Ma}}{dt}\\[2mm]\dfrac{dq_{nm2\_Mi}}{dt}\\[2mm]\dfrac{dq_{fn}}{dt}\\[2mm]\dfrac{dq_{Fn}}{dt}\end{bmatrix}=(2n-1)^2\begin{bmatrix}-\left(\dfrac{1}{\tau_{m1}}+\dfrac{T_{Fm1}}{\tau_F J_F}\right)&0&-\dfrac{T_{Fm1}}{\tau_F J_F}&\dfrac{T_{Fm1}}{\tau_F J_F}\\[2mm]0&-\left(\dfrac{1}{\tau_{m2}}+\dfrac{T_{fm2}}{\tau_f T_{Ff}}\right)&\dfrac{T_{fm2}}{\tau_f T_{Ff}}&0\\[2mm]\dfrac{1}{\tau_F}&-\dfrac{T_{Ff}}{\tau_F J_F}&-\left(\dfrac{1}{\tau_f}+\dfrac{T_{Ff}}{\tau_F J_F}\right)&\dfrac{T_{Ff}}{\tau_F J_F}\\[2mm]0&\dfrac{1}{\tau_F}&\dfrac{1}{\tau_F}&\dfrac{1}{\tau_F}\end{bmatrix}\begin{bmatrix}C_1 q_{nm1\_Ma}\\[1mm]C_2 q_{nm2\_Mi}\\[1mm]q_{fn}\\[1mm]q_{Fn}\end{bmatrix}.$$

(B9)

For this coefficient matrix in Eq. (B9), we obtain four eigenvalues, namely, λ_1, λ_2, λ_3, λ_4 and four eigenvectors, namely, $\xi_1, \xi_2, \xi_3, \xi_4$ and r_1-r_{16} represent the elements in eigenvectors.

$$\xi_1=\begin{pmatrix}r_1\\r_2\\r_3\\r_4\end{pmatrix},\ \xi_2=\begin{pmatrix}r_5\\r_6\\r_7\\r_8\end{pmatrix},\ \xi_3=\begin{pmatrix}r_9\\r_{10}\\r_{11}\\r_{12}\end{pmatrix},\ \xi_4=\begin{pmatrix}r_{13}\\r_{14}\\r_{15}\\r_{16}\end{pmatrix}.$$

(B10)

The fluid flow has not yet occurred in the matrix and microfracture when time $t=0$ and the initial production rate depends on the contribution from macrofractures, which is defined as q_{Fin}.

$$q_{nm1\_Ma}(t=0)=0,$$

(B11)

$$q_F = \beta_1\beta_3 r_4 q_{Fin}e^{\lambda_1 t} + \beta_1\beta_2 r_8 q_{Fin}e^{\lambda_2 t} - \beta_1\alpha_4 r_{12} q_{Fin}e^{\lambda_3 t}$$
$$+\beta_1\alpha_3 r_{16}q_{Fin}e^{\lambda_4 t}+\sum_{n=2}^{\infty}\Big(\beta_1\beta_3 r_4 q_{Fin}e^{(2n-1)^2\lambda_1 t}$$
$$+\beta_1\beta_2 r_8 q_{Fin}e^{(2n-1)^2\lambda_2 t}-\beta_1\alpha_4 r_{12} q_{Fin}e^{(2n-1)^2\lambda_3 t}$$
$$+\beta_1\alpha_3 r_{16}q_{Fin}e^{(2n-1)^2\lambda_4 t}\Big).$$

(B15)

We define $Z=(2n-1)\sqrt{|\lambda_1 t|}$ and calculate the derivative as

$$dn=\frac{dZ}{2\sqrt{|\lambda_1 t|}}.$$

(B16)

Therefore, Eq. (B15) can convert the summation to an integral:

$$q_F = \beta_1\beta_3 r_4 q_{Fin}e^{\lambda_1 t}+\beta_1\beta_2 r_8 q_{Fin}e^{\lambda_2 t}-\beta_1\alpha_4 r_{12}q_{Fin}e^{\lambda_3 t}+\beta_1\alpha_3 r_{16}q_{Fin}e^{\lambda_4 t}$$
$$+\lim_{z\to\infty}\int_{3\sqrt{|\lambda_1 t|}}^{Z}\left(\beta_1\beta_3 r_4 q_{Fin}e^{z^2}+\beta_1\beta_2 r_8 q_{Fin}e^{\frac{\lambda_2}{|\lambda_1|}z^2}-\beta_1\alpha_4 r_{12}q_{Fin}e^{\frac{\lambda_3}{|\lambda_1|}z^2}+\beta_1\alpha_3 r_{16}q_{Fin}e^{\frac{\lambda_4}{|\lambda_1|}z^2}\right)\frac{dZ}{2\sqrt{|\lambda_1 t|}}.$$

(B17)

$$q_{nm2\_Mi}(t=0)=0,$$

(B12)

By adopting the error function, Eq. (B17) can be valuated and simplified as

$$q_{\mathrm{F}} = \beta_1\beta_3 r_4 q_{\mathrm{Fin}}\mathrm{e}^{\lambda_1 t} + \beta_1\beta_2 r_8 q_{\mathrm{Fin}}\mathrm{e}^{\lambda_2 t} - \beta_1\alpha_4 r_{12} q_{\mathrm{Fin}}\mathrm{e}^{\lambda_3 t} + \beta_1\alpha_3 r_{16} q_{\mathrm{Fin}}\mathrm{e}^{\lambda_4 t}$$

$$+ \frac{q_{\mathrm{Fin}}}{2\sqrt{|\lambda_1 t|}}\lim_{z\to\infty}\left(\begin{array}{l} \beta_1\beta_3 r_4 \dfrac{\sqrt{\pi}}{2}\mathrm{erf}(z) + \beta_1\beta_2 r_8 \left|\dfrac{\lambda_1}{\lambda_2}\right|\dfrac{\sqrt{\pi}}{2}\mathrm{erf}\left(\sqrt{\left|\dfrac{\lambda_2}{\lambda_1}\right|}z\right) \\[4mm] -\beta_1\alpha_4 r_{12}\left|\dfrac{\lambda_1}{\lambda_3}\right|\dfrac{\sqrt{\pi}}{2}\mathrm{erf}\left(\sqrt{\left|\dfrac{\lambda_3}{\lambda_1}\right|}z\right) + \beta_1\alpha_3 r_{16}\left|\dfrac{\lambda_1}{\lambda_4}\right|\dfrac{\sqrt{\pi}}{2}\mathrm{erf}\left(\sqrt{\left|\dfrac{\lambda_4}{\lambda_1}\right|}z\right) \end{array}\right)\Bigg|_{3\sqrt{|\lambda_1 t|}}^{z} \tag{B18}$$

For the limit, when $z\to\infty$, $\lim\limits_{z\to\infty}\mathrm{erf}(z) = 1$. And for the complementary error function can be written as $\mathrm{erfc}(z) = 1 - \mathrm{erf}(z)$.

Finally, the approximate analytical solution can be derived as

$$q_{\mathrm{F}} = \beta_1\beta_3 r_4 q_{\mathrm{Fin}}\mathrm{e}^{\lambda_1 t} + \beta_1\beta_2 r_8 q_{\mathrm{Fin}}\mathrm{e}^{\lambda_2 t} - \beta_1\alpha_4 r_{12} q_{\mathrm{Fin}}\mathrm{e}^{\lambda_3 t}$$

$$+ \beta_1\alpha_3 r_{16} q_{\mathrm{Fin}}\mathrm{e}^{\lambda_4 t} + \frac{\sqrt{\pi}\beta_1\beta_3 r_4 q_{\mathrm{Fin}}}{4\sqrt{|\lambda_1 t|}}\mathrm{erfc}\left(3\sqrt{|\lambda_1 t|}\right)$$

$$+ \frac{\sqrt{\pi}\beta_1\beta_2 r_8 q_{\mathrm{Fin}}}{4\sqrt{|\lambda_2 t|}}\mathrm{erfc}\left(3\sqrt{|\lambda_2 t|}\right)$$

$$- \frac{\sqrt{\pi}\beta_1\alpha_4 r_{12} q_{\mathrm{Fin}}}{4\sqrt{|\lambda_3 t|}}\mathrm{erfc}\left(3\sqrt{|\lambda_3 t|}\right)$$

$$+ \frac{\sqrt{\pi}\beta_1\alpha_3 r_{16} q_{\mathrm{Fin}}}{4\sqrt{|\lambda_4 t|}}\mathrm{erfc}\left(3\sqrt{|\lambda_4 t|}\right). \tag{B19}$$

References

Abdassah, D., Ershaghi, I., 1986. Triple-porosity systems for representing naturally fractured reservoirs. SPE Form. Eval. 1 (2), 113–127. https://doi.org/10.2118/13409-PA.

Alahmadi, H.A.H., 2010. A Triple-Porosity Model for Fractured Horizontal Wells. Master Thesis. Texas A & M University, TX.

Al-Ghamdi, A., Ershaghi, I., 1996. Pressure transient analysis of dually fractured reservoirs. SPE J. 1 (1), 93–100. https://doi.org/10.2118/26959-PA.

Ali, A.J., Siddiqui, S., Dehghanpour, H., 2013. Analyzing the production data of fractured horizontal wells by a linear triple porosity model: development of analysis equations. J. Petrol. Sci. Eng. 112, 117–128. https://doi.org/10.1016/j.petrol.2013.10.016.

Al-Rbeawi, S., 2018. Bivariate log-normal distribution of stimulated matrix permeability and block size in fractured reservoirs: proposing new multilinear-flow regime for transient-state production. SPE J. 23 (4), 1316–1342. https://doi.org/10.2118/189993-PA.

Barenblatt, G., Zheltov, l.P., Kochina, I., 1960. Basic concepts in the theory of seepage of homogeneous liquids in fissured rocks [strata]. J. Appl. Math. Mech. 24 (5), 1286–1303. https://doi.org/10.1016/0021-8928(60)90107-6.

Behmanesh, H., Anderson, D.M., Thompson, J.M., et al., 2017. An improved practical solution for modeling single phase multi-fractured horizontal well performance. In: SPE Unconventional Resources Conference. https://doi.org/10.2118/185063-MS.

Bello, R.O., 2009. Rate Transient Analysis in Shale Gas Reservoirs with Transient Linear Behavior. PhD Dissertation. Texas A&M University, TX.

Brown, M., Ozkan, E., Raghavan, R., Kazemi, H., 2011. Practical solutions for pressure-transient responses of fractured horizontal wells in unconventional shale reservoirs. SPE Reservoir Eval. Eng. 14 (6), 663–676. https://doi.org/10.2118/125043-PA.

Clarkson, C.R., Pedersen, P.K., 2011. Production analysis of western Canadian unconventional light oil plays. In: Canadian Unconventional Resources Conference. https://doi.org/10.2118/149005-MS.

De Swaan, O.A., 1976. Analytic solutions for determining naturally fractured reservoir properties by well testing. SPE J. 16 (3), 117–122. https://doi.org/10.2118/5346-PA.

Dehghanpour, H., Shirdel, M., 2011. A triple porosity model for shale gas reservoirs. In: Canadian Unconventional Resources Conference. https://doi.org/10.2118/149501-MS.

Dreier, J., 2004. Pressure-transient Analysis of Wells in Reservoirs with a Multiple Fracture Network. Master Thesis. Colorado School of Mines, CO.

El-Banbi, A., 1998. Analysis of Tight Gas Well Performance. PhD Dissertation. Texas A&M University, TX.

Ezulike, D.O., Dehghanpour, H., 2014. A model for simultaneous matrix depletion into natural and hydraulic fracture networks. J. Nat. Gas Sci. Eng. 16, 57–69. https://doi.org/10.1016/j.jngse.2013.11.004.

Kazemi, H., 1969. Pressure transient analysis of naturally fractured reservoirs with uniform fracture distribution. SPE J. 9 (4), 451–462. https://doi.org/10.2118/2156-A.

Lu, Y.H., Wei, S.M., Xia, Y., et al., 2021. Modeling of geomechanics and fluid flow in fractured shale reservoirs with deformable multi-continuum matrix. J. Petrol. Sci. Eng. 196, 107576. https://doi.org/10.1016/j.petrol.2020.107576.

Ogunyomi, B.A., Patzek, T.W., Lake, L.W., et al., 2016. History matching and rate forecasting in unconventional oil reservoirs with an approximate analytical solution to the double-porosity model. SPE Reservoir Eval. Eng. 19 (1), 70–82. https://doi.org/10.2118/171031-PA.

Qiu, K.X., 2023. A practical analytical model for performance prediction in unconventional gas reservoir. Front. Earth Sci. 11, 1143541. https://doi.org/10.3389/feart.2023.1143541.

Qiu, K.X., Li, H., 2019. A new analytical model for production forecasting in unconventional reservoir considering the simultaneous matrix-fracture flow. In: Asia Pacific Unconventional Resources Technology Conference. https://doi.org/10.15530/AP-URTEC-2019-198266.

Rafael, R.N., Héber, C.L., Fernando, S.V., 2002. Fractured reservoir parameters estimation considering multiple block size. In: SPE International Petroleum Conference and Exhibition. https://doi.org/10.2118/74387-MS.

Samandarli, O., 2012. A New Method for History Matching and Forecasting Shale Gas/oil Reservoir Production Performance with Dual and Triple Porosity Models. Master Thesis. Texas A & M University, TX.

Segall, P., 1981. Development of Joints and Faults of Granitic Rocks. PhD Dissertation. Stanford University, CA.

Stalgorova, E., Mattar, L., 2012. Practical analytical model to simulate production of horizontal wells with branch fractures. In: SPE Canadian Unconventional Resources Conference. https://doi.org/10.2118/162515-MS.

Stalgorova, K., Mattar, L., 2013. Analytical model for unconventional multifractured composite systems. SPE Reservoir Eval. Eng. 16 (3), 246–256. https://doi.org/10.2118/162516-PA.

Stehfest, H., 1970. Algorithm 368: numerical inversion of Laplace transforms [D5]. Commun. ACM 13 (1), 47–49. https://dl.acm.org/doi/pdf/10.1145/361953.361969.

Tivayanonda, V., 2012. Comparison of Single, Double, and Triple Linear Flow Models for Shale Gas/oil Reservoirs. Master Thesis. Texas A & M University, TX.

Wang, Y., Ayala, L.F., 2020. Explicit determination of reserves for variable-bottomhole-pressure conditions in gas rate-transient analysis. SPE J. 25 (1), 369–390. https://doi.org/10.2118/195691-PA.

Warren, J., Root, P.J., 1963. The behavior of naturally fractured reservoirs. SPE J. 3 (3), 245–255. https://doi.org/10.2118/426-PA.

Wattenbarger, R.A., El-Banbi, A.H., Villegas, M.E., et al., 1998. Production analysis of linear flow into fractured tight gas wells. In: SPE Rocky Mountain Regional/low-Permeability Reservoirs Symposium.

Wei, S.M., Xia, Y., Jin, Y., et al., 2019. Quantitative study in shale gas behaviors using a coupled triple-continuum and discrete fracture model. J. Petrol. Sci. Eng. 174, 49–69. https://doi.org/10.1016/j.petrol.2018.10.084.

Wu, Y.H., Cheng, L.S., Huang, S.J., et al., 2019. An analytical model for analyzing the impact of fracturing fluid-induced formation damage on rate transient behavior in tight formations. J. Petrol. Sci. Eng. 179, 513–525. https://doi.org/10.1016/j.petrol.2019.04.090.

Wu, Y.H., Cheng, L.S., Ma, L.Q., et al., 2021. A transient two-phase flow model for production prediction of tight gas wells with fracturing fluid-induced formation damage. J. Petrol. Sci. Eng. 199, 108351. https://doi.org/10.1016/j.petrol.2021.108351.

Wu, Y.H., Fang, S.D., Wang, S.R., et al., 2023. A novel production data analysis method for multi-fractured horizontal wells with infill well-caused fracture interference. Petrol. Sci. 20 (5). https://doi.org/10.1016/j.petsci.2023.04.002.